Observer-Based Event-Triggered Sliding Mode Control for Secure Formation Tracking of Multi-UAV Systems

Tingting Yin, Zhou Gu, *Member, IEEE*, and Xiangpeng Xie, *Member, IEEE*

***Abstract*—This article is concerned with the problem of the secure formation tracking of multiple unmanned aerial vehicles (UAVs) subject to replay attacks, where an observer-based event-triggered sliding mode control approach is adopted. First, a novel attack model is established for multi-UAV systems considering replay attacks, in which the issue of the replay attack beginning and ending within a sampling period is solved. Then, a switched event-triggered scheme is developed for multi-UAV systems subject to replay attacks, under which the corresponding communication mechanisms are invoked for different attack states. This communication scheme brings lower data releasing rate and less energy consumption based on the severity level of replay attacks while the desired tracking performance is ensured. On the basis of the sliding mode control theory, observer-based event-triggered formation tracking strategies are developed for multi-UAV systems with nonlinearities under replay attacks by combining the interactive information from neighbors. Sufficient conditions of the multi-UAV system to achieve the desired formation are obtained by utilizing Lyapunov stability approach. Finally, a simulation example with multiple UAVs is performed to demonstrate the validity of the developed formation control strategy.**

***Index Terms*—Event-triggered scheme, formation tracking control, replay attacks, sliding mode control, unmanned aerial vehicles.**

I. Introduction

The past decades have witnessed significant progress in the development of unmanned aerial vehicles (UAVs). They have the advantages of light weight, compact size, low cost, and flying ability in severe environments, thereby easily meeting requirements for a multitude of applications, such as forest fire detection [1], radiation detection, and contour mapping [2], and express delivery for long distances and/or large differences in height. However, a single UAV has many shortcomings in completing complex missions. For instance, a single UAV may be unable to observe the objective from different directions because of the sensor's detection limitation when conducting a reconnaissance task. To address this problem, the cooperativity among multiple UAVs is of great indispensability. Regarded as one representative for cooperative control technologies, the formation tracking control of multiple UAVs has attracted considerable interest over the past years [3], [4], [5], [6], [7], [8] and the references therein. For example, formation tracking control strategies were developed for multi-UAV systems with switching directed topologies [9], [10] and velocity constraints [11]. The authors in [12] investigated the tracking control issue for multi-UAV systems with the method of sliding mode control (SMC). The main advantages of SMC include fast response, easy tuning and implementation, high robustness, and good transient performance [13], [14], [15]. Extensive attention has been paid to SMC technique in recent years [16], [17]. To our knowledge, the formation control issue for multi-UAV systems has not been fully studied, especially in unknown aerodynamics and nonlinearities. Therefore, it is meaningful and challenging to investigate the formation tracking control for multi-UAV systems with nonlinearities using the SMC method. This is the main motivation for this research.

In a multi-UAV system, to accomplish the assigned missions efficiently and effectively, it is essential to realize reliable information delivery among UAVs through a wireless communication network. As a consequence, the network plays a significant role in the formation flight of multiple UAVs. However, the openness and sharing of the network result in the multi-UAV system being available to security threats, such as network-introduced delay, packet loss, and cyber-attack, etc. Regarding the network security issue, the most important characteristic considered in a multi-UAV system is to operate resiliently and maintain the UAV tracking performance even during nonlinearities and cyber-attacks. Any successful attack may significantly degrade system performance or even lead to system paralysis. The research community has acknowledged the significance of handling the challenge of developing secure estimation, detection, and control systems with cyber-attacks. Several types of cyber-attacks have been studied in [18], [19], [20], [21], [22], including denial-of-service (DoS) attacks, deception attacks, and replay attacks. Among these attacks, replay attacks are regarded as a class of much more common and natural cyber-attacks. Replay attackers launch an attack by maliciously

Manuscript received 5 September 2022; revised 28 October 2022; accepted 19 November 2022. Date of publication 23 November 2022; date of current version 23 February 2023. This work was supported by the National Natural Science Foundation of China under Grants 62273183 and 62022044. Recommended for acceptance by Dr. Xiang Li. *(Corresponding author: Zhou Gu.)*

Tingting Yin and Zhou Gu are with the College of Mechanical and Electronic Engineering, Nanjing Forestry University, Nanjing 210037, China (e-mail: yttangle@163.com; gzh1808@163.com).

Xiangpeng Xie is with the Institute of Advanced Technology, Nanjing University of Posts and Telecommunications, Nanjing 210023, China (e-mail: xiexiangpeng1953@163.com).

Digital Object Identifier 10.1109/TNSE.2022.3223978

repeating the transmitted data in the past period, thereby causing the degradation of the system performance. An enormous number of results involving replay attacks have been obtained in the past decades, see [23], [24], [25], [26], [27] and the references therein. For example, the authors in [23] developed a formal security analysis and old-fashioned cryptanalysis, which was resilient against replay attacks. The problem of the speed synchronization control was addressed for a connected vehicle under replay attacks in [24], where the replay attack was depicted by large random network delays. The consensus control strategy for multiagent systems was proposed in [28] in the presence of replay attacks. In [28], the occurrence of replay attacks was governed by a Bernoulli variable, which means that the transmitted signals are replaced by packets at some past discrete instants when the system is subject to replay attacks. In fact, for replay attacks, adversaries maliciously or fraudulently repeat the data transmitted in the past period to degrade the system performance. Therefore, it is unreasonable to model replay attacks by simply introducing a Bernoulli variable. Note that few published achievement is concerned with multi-UAV systems under cyber-attacks, although cyber-attacks pose a great threat to the communication security among UAVs. Accordingly, it is necessary and challenging to explore the description and modeling methods of such replay attacks in multi-UAV systems. This is another motivation of this study.

On the other hand, due to the limitation of network resources, plenty of efforts have been devoted to improving resource utilization such that the network load could be eased without compromising the desired system performance [29], [30], [31], [32], [33], [34]. Event-triggered scheme (ETS) has received extensive attention in the past years owing to its advantages over periodic sampling control (that is time-triggered scheme), see [35], [36], [37], [38], [39]. Specifically, in the ETS, control tasks are executed according to some events generated by state-dependent triggering conditions rather than the elapse of a certain period as in the time-triggered scheme. Besides, ETS brings aperiodic updates of sampling signals, thereby leading to more flexibility to manage constraints based on networks and systems interactions than a time-triggered scheme. More exactly, the periodic execution of control tasks in the time-triggered scheme is usually undesirable because of the communication bandwidth constraint. To develop the ETS, a crucial step is to design suitable triggering conditions for deciding whether sampling data should be transmitted or not. The triggering conditions with fixed thresholds were proposed for the ETS in [40], [41], and hence largely saved the limited network resources. The authors in [42] concentrated on the reinforcement learning control for the quadrotor UAV by using such an ETS. Over the last few years, the event-triggered mechanism with predefined thresholds has been improved. In [43], a hybrid-triggered mechanism was developed, where the time-triggered scheme and event-triggered scheme were randomly switched based on a Bernoulli variable. The authors in [32] proposed a new adaptive event-triggering scheme, in which the triggering threshold could be dynamically adapted according to the variation of system states. In [44], a memory-based event-triggered scheme based on both the current and past information of system states was put forward, by which the wrong data-releasing event caused by sudden state changes was reduced. The authors proposed a resilient ETS in [19] to mitigate the impacts of DoS attacks and a switched ETS in [21] for deception attacks. However, it is a challenging issue to design an appropriate event-triggered scheme to further save network capital and guarantee the performance of multi-UAV systems subject to replay attacks, which is also a motivation of this study.

Motivated by the aforementioned discussion, we mainly investigate the issue of the observer-based event-triggered sliding mode control for formation tracking of multi-UAV systems subject to replay attacks. The main contributions of this study are presented in the following aspects:

1) A new model of replay attacks is constructed for multi-UAV systems, under which each attack period is divided into sleeping and active periods. The data transmission is normal in sleeping periods; in active periods, the packets during the current period are replaced by those during a certain period in the past. Compared to research on replay attacks described by Bernoulli variables [28], this attack model describes the replay attacker's behavior more reasonably and accurately.
2) A novel switched ETS is proposed for multi-UAV systems with replay attacks to address the off/on (on/off) transitions of replay attacks occurring within a sampling period. Compared with the event-triggered scheme in [28], the proposed communication scheme can dynamically switch according to different attack states, by which the redundant data can be greatly reduced while the performance of the multi-UAV system is kept to be a prescribed level.
3) Based on the sliding mode control theory, an event-triggered formation tracking control strategy with an observer-based sliding mode approach is developed for multi-UAV systems with nonlinearities and replay attacks. By applying the Lyapunov stability theory, sufficient conditions of the multi-UAV system to achieve the desired formation are acquired. At last, a simulation example is presented to testify the validity of the proposed formation control strategies.

Notation: $\mathrm{col}_N\{\cdot\}$ represents N-columns vector; $\mathrm{col}_N^i\{\cdot\}$ denotes N-columns vector only with the i-th column is nonzero. I_N stands for the $(N \times N)$-dimensional identity matrix which is abbreviated as I sometimes. $\lambda_{\mathrm{M}}(X)$ and $\lambda_{\mathrm{m}}(X)$ denote the maximum eigenvalue and the minimum eigenvalue of matrix X, respectively. $\mathrm{sym}\{X\}$ denotes $X + X^T$. $\mathbb{R}^{n_1 \times n_2}$ and $\mathbb{R}^{n_1}$ are the set of $n_1 \times n_2$ real matrices and n_1-dimensional Euclidean space, respectively.

II. System Modeling and Problem Description

A. Basic Graph Theory

The directed graph $\mathbf{F} = (\mathbf{V}, \mathbf{E}, \mathbf{W})$ describes the communication topology among N UAVs, where $\mathbf{E} \subseteq \{(i,j), i,j \in \mathbf{V}\}$ and $\mathbf{V} \in \{1, 2, \ldots, N\}$ indicate the set of edges and nodes, respectively. $\mathbf{W} = [w_{ij}]$ is the weighted adjacency of $\mathbf{F}$, where

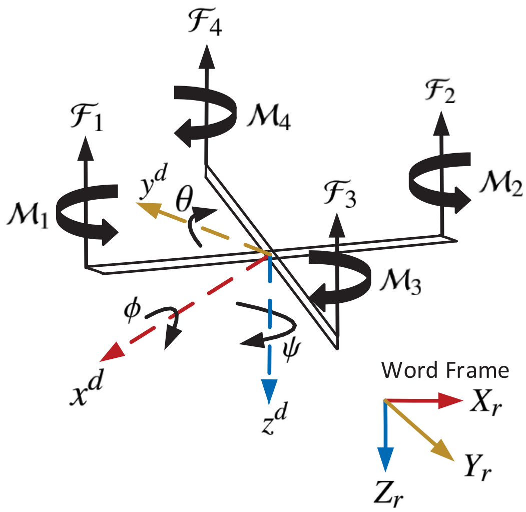

Fig. 1. Diagram of the quadrotor UAV in its body frame.

$w_{ii} = 0$, $w_{ij} = 1 \Leftrightarrow (j,i) \in \mathbf{E}$; otherwise, $w_{ij} = 0$. Edge $(j,i) \in \mathbf{E}$ means that the i-th UAV can receive the j-th UAV's information. Denote $\mathcal{Z}_i = \{j|(i,j) \in \mathbf{E}\}$ as the set containing all adjacent UAVs for the i-th UAV. The Laplacian matrix is represented as $\mathrm{L} = [\mathfrak{L}_{ij}]$, in which $\mathfrak{L}_{ii} = \Sigma_{j\neq i} w_{ij}$, $\mathfrak{L}_{ij} = -w_{ij}$ for $i \neq j$, $i,j \in \mathbf{V}$.

B. Dynamic Model of a Quadrotor UAV

The flight motion of a quadrotor UAV includes translational motion and rotational motion [8], [38]. In what follows, the control model of the UAV will be established from these two parts.

1) Translational Motion: Applying Newton's second law yields that

$$\begin{bmatrix} \ddot{X}_r \\ \ddot{Y}_r \\ \ddot{Z}_r \end{bmatrix} = \mathcal{W}_r \begin{bmatrix} 0 \\ 0 \\ -\frac{u_{to}}{m} \end{bmatrix} + \begin{bmatrix} 0 \\ 0 \\ \mathbf{g}_r \end{bmatrix}, \tag{1}$$

where $u_{to} = \mathcal{F}_1 + \mathcal{F}_2 + \mathcal{F}_3 + \mathcal{F}_4$ is the total thrust, in which $\mathcal{F}_p$, $p \in \{1,2,3,4\}$ stand for the lifts produced by four motors exhibited in Fig. 1; m and $\mathbf{g}_r$ are the mass of the UAV and the acceleration of gravity, respectively. In the world frame, the East, North, and Down positions of UAV are represented as Y_r, X_r, and Z_r, respectively. In Fig. 1, θ, ϕ, ψ denote the pitch, roll, and yaw angles, respectively. The transition matrix $\mathcal{W}_{tr}$ can realize the coordinate transition from the body frame to the world frame for the UAV, which is defined as

$$\mathcal{M} = \begin{bmatrix} \mathcal{C}_\theta \mathcal{C}_\psi & \mathcal{C}_\psi \mathcal{S}_\phi \mathcal{S}_\theta - \mathcal{C}_\phi \mathcal{S}_\psi & \mathcal{S}_\phi \mathcal{S}_\psi + \mathcal{C}_\phi \mathcal{C}_\psi \mathcal{S}_\theta \\ \mathcal{C}_\theta \mathcal{S}_\psi & \mathcal{C}_\phi \mathcal{C}_\psi + \mathcal{S}_\phi \mathcal{S}_\theta \mathcal{S}_\psi & \mathcal{C}_\phi \mathcal{S}_\theta \mathcal{S}_\psi - \mathcal{C}_\psi \mathcal{S}_\theta \\ -\mathcal{S}_\phi & \mathcal{C}_\theta \mathcal{S}_\phi & \mathcal{C}_\phi \mathcal{C}_\theta \end{bmatrix},$$

with $\mathcal{C}_{(\cdot)}$ and $\mathcal{S}_{(\cdot)}$ denoting $\cos(\cdot)$ and $\sin(\cdot)$ respectively.

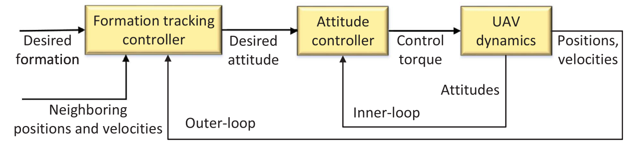

Fig. 2. Control strategy of the UAV.

Taking $\mathcal{W}_{tr}$ into (1) yields that

$$\begin{cases} \ddot{X}_r = \frac{u_{to}}{m}(-\mathcal{S}_\phi \mathcal{S}_\psi - \mathcal{C}_\phi \mathcal{S}_\theta \mathcal{C}_\psi), \\ \ddot{Y}_r = \frac{u_{to}}{m}(\mathcal{S}_\phi \mathcal{C}_\psi - \mathcal{C}_\phi \mathcal{S}_\theta \mathcal{S}_\psi), \\ \ddot{Z}_r = \mathbf{g}_r - \frac{u_{to}}{m} \mathcal{C}_\phi \mathcal{C}_\theta. \end{cases} \tag{2}$$

2) Rotational Motion: Utilizing Euler's equations follows that

$$\mathfrak{I} = \mathbb{I}\dot{\Upsilon} + \Upsilon \times \mathbb{I}\Upsilon, \tag{3}$$

where $\Upsilon = [r_x, r_y, r_z]^T$ represents the UAV's angular velocity in its body-fixed frame; $\mathfrak{I}$ is the UAV's total moment; $\mathbb{I}$ is the inertial tensor matrix, which is treated as a diagonal matrix owing to the symmetry of the layout for the quadrotor UAV. $\mathcal{M}_p$, $p \in \{1,2,3,4\}$ are the torques of four motors shown in Fig. 1. More details of rotational motion for the quadrotor UAV can be found in [13].

When the UAV flight is near the hover state, $u_{to} \approx m\mathbf{g}_r$, $\phi \approx 0$, $\theta \approx 0$, $\dot{\phi} \approx 0$ and $\dot{\theta} \approx 0$. Then, the following linearized model of the quadrotor UAV near the hover can be acquired according to (2).

$$\begin{cases} \ddot{X}_r = \mathbf{g}_r(-\phi \mathcal{S}_\psi - \theta \mathcal{C}_\psi), \\ \ddot{Y}_r = \mathbf{g}_r(-\theta \mathcal{S}_\psi + \phi \mathcal{C}_\psi), \\ \ddot{Z}_r = \frac{u_{to} - m\mathbf{g}_r}{m}. \end{cases} \tag{4}$$

Remark 1: From (4), one can see that the control of the UAV, including its own altitude and three-axis attitude control, is entirely decoupled [13], which brings that the quadrotor UAV system could be independently controlled for its flight and formation.

Fig. 2 exhibits the inner-loop and outer-loop control mechanisms for the quadrotor UAV. It is well-known that the inner-loop control is realized through a PD controller while the outer-loop is dependent on a formation tracking controller. This study will concentrate on the problem of the formation tracking control of multiple UAVs in the following.

C. Multi-UAV System Modeling

Consider a multi-UAV system with one leader (labeled as the 0-th UAV) and N followers (labeled as $1, 2, \ldots, N$). Define $x_i(t) = [\,\zeta_i(t) \quad v_i(t)\,]^T$, where $\zeta_i(t) \in \mathbb{R}^q$ and $v_i(t) = \dot{\zeta}_i(t)$ $(i = 0, 1, 2 \cdots, N)$ denote the position and the velocity, respectively. For convenience, let $q = 1$ in what follows. Then, the dynamic equations of the 0-th UAV and the i-th follower are described as

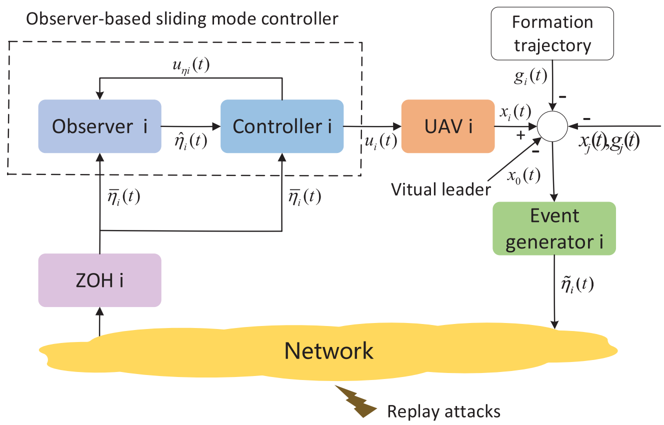

Fig. 3. Diagram of the event-triggered control for the i-th UAV.

$$\dot{x}_0(t) = Ax_0(t) + Bu_0(t), \tag{5}$$
$$\dot{x}_i(t) = Ax_i(t) + Bu_i(t) + Ud_i(t), \tag{6}$$

where $A = \begin{bmatrix} 0 & 1 \\ 0 & 0 \end{bmatrix}$, $B = \begin{bmatrix} 0 \\ 1 \end{bmatrix}$, and U is a real constant matrix; $u_i(t)$ is the i-th UAV's control input, $i = 1, 2, \ldots, N$; $u_0(t) = \dot{v}_0(t)$. The nonlinear function $d_i(t)$ denotes the aggregation of various nonlinear behaviors that satisfies $\|d_i(t)\|_2 \leq \|Fx_i(t)\|_2$, where F is a matrix of suitable dimension. All the results hereafter could be directly extended to the situation of $q \geq 2$ by applying the Kronecker product.

Assumption 1: The directed communication topology **F** has a directed spanning tree with the 0-th UAV served as its root node.

The time-varying formation for followers is described by $g(t) = [g_1^T(t), g_2^T(t), \ldots, g_N^T(t)]^T$, where $g_i(t) = [g_{i\zeta}(t), g_{iv}(t)]^T$ $(i \in \{1, 2, \ldots, N\} \triangleq \mathbb{J}_N)$ is the continuously differentiable formation vector, in which $g_{i\zeta}(t)$ $(g_{iv}(t))$ denotes the position (velocity) of the i-th UAV, and $g_{iv}(t) = \dot{g}_{i\zeta}(t)$.

Define the tracking error for the i-th UAV $(i \in \mathbb{J}_N)$ as

$$\eta_i(t) = \sum_{j \in \mathcal{Z}_i} w_{ij}[\breve{x}_i(t) - \breve{x}_j(t)] + a_i[\breve{x}_i(t) - x_0(t)], \tag{7}$$

where $\breve{x}_i(t) = x_i(t) - g_i(t)$; $a_i = 1$ denotes that the i-th UAV can receive the information of the leader (namely, the 0-th UAV); otherwise, $a_i = 0$.

Calculating the derivation of (7) follows that

$$\dot{\eta}_i(t) = A\eta_i(t) + Bu_{\eta i}(t) + U\tilde{d}_i(t), \tag{8}$$

where $u_{\eta i}(t)$ is the formation control input, which satisfies $Bu_{\eta i}(t) = \sum_{j \in \mathcal{Z}_i} w_{ij}[Bu_i(t) + Ag_i(t) - \dot{g}_i(t) - Bu_j(t) - Ag_j(t) + \dot{g}_j(t)] + a_i[Bu_i(t) - Bu_0(t) + Ag_i(t) - \dot{g}_i(t)]$, $\tilde{d}_i(t) = \sum_{j \in \mathcal{Z}_i} w_{ij}[d_i(t) - d_j(t)] + a_i d_i(t)$. The relationship between the nonlinear function $\tilde{d}_i(t)$ and the tracking error $\eta_i(t)$ is assumed to satisfy the following constraint: $\|\tilde{d}_i(t)\|_2 \leq \|\tilde{F}\eta_i(t)\|_2$ with the matrix $\tilde{F}$ of appropriate dimension.

D. Replay Attacks

As shown in Fig. 3, replay attacks are considered in this study. When replay attacks occur, the signals transmitted in the past period are maliciously repeated or delayed. Due to the limitation of power, attackers need sleep during a certain period to save energy. Denote h as the sampling step of the i-th UAV's state, then, the transmitted data via the network with replay attacks can be expressed as

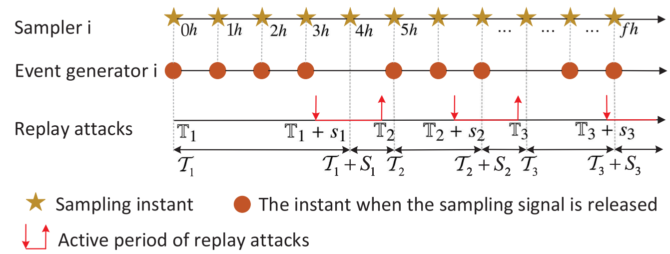

Fig. 4. Time sequence of the system under replay attacks and event-triggered scheme.

$$\bar{\eta}_i(t) = \begin{cases} \tilde{\eta}_i(t), & t \in [\mathcal{T}_n, \mathcal{T}_n + S_n), \\ \tilde{\eta}_i(t - \varepsilon), & t \in [\mathcal{T}_n + S_n, \mathcal{T}_{n+1}), \end{cases} \tag{9}$$

where $\mathcal{T}_n = (\lfloor \mathbb{T}_n/h \rfloor + 1)h$, $S_n = (\lfloor (\mathbb{T}_n + s_n)/h \rfloor + 1)h - \mathcal{T}_n$ with s_n denoting the sleeping time of the attack in an attack period $[\mathbb{T}_n, \mathbb{T}_{n+1})$; $0 \leq \mathbb{T}_n < \mathbb{T}_n + s_n < \mathbb{T}_{n+1}$, $n \in \mathcal{N}$, $\mathcal{N}$ stands for the set of positive integers; $\varepsilon \geq 0$ is a constant. For the convenience of mathematical expression, we denote $F_n^1 = [\mathcal{T}_n, \mathcal{T}_n + S_n)$ and $F_n^2 = [\mathcal{T}_n + S_n, \mathcal{T}_{n+1})$ as the sleeping period and active period of replay attacks, respectively. In this study, it is assumed that the replay attack can be detected via technical methods, such as the attck detection mechanism based on Bayesian inference in [25], the power-based intrusion detection method in [26].

Remark 2: In this study, each replay attack period is divided into sleeping and active periods. An attack in the sleeping period represents the signal transmission is normal, while an attack in the active period denotes the attacker replacing packets during the current period with those during a certain period in the past. The system at different periods has different dynamics. Consequently, it can be modeled by using the switched system (9). Compared to the replay attack model in [28], our built model of replay attacks in this study is more reasonable and accurate, thus it has more practical significance.

Remark 3: In (9), one can observe that the definitions of $\mathcal{T}_n$ and S_n are based on the sampling step h due to the use of the event-triggered mechanism. To help understand this, we present Fig. 4to show the time sequence of replay attacks. For instance, if the replay attack occurs between the third and fourth sampling instant, the fourth sampling instant is treated as the beginning of the active period.

For a normal system, if it is attacked for a long time, the stability and reliability of the system will be affected. Therefore, we make the following reasonable assumption and definition:

Assumption 2: In $[0, t)$, one can always find a positive scalar $\mathcal{T}_M$ for F_n^2 satisfying

$$\sup_{n \in \mathcal{N}} \{\mathcal{T}_{n+1} - \mathcal{T}_n - S_n\} \leq \mathcal{T}_M, \tag{10}$$

and a positive scalar $\mathcal{T}_m$ for F_n^1 satisfying

$$\inf_{n\in\mathcal{N}}\{S_n\} \geq \mathcal{T}_m. \tag{11}$$

Remark 4: From Assumption 2, one can get that there exists a uniform upper bound $\mathcal{T}_M$ on length of active period $\mathcal{T}_{n+1} - \mathcal{T}_n - S_n$ and a uniform lower bound $\mathcal{T}_m$ on length of sleeping period S_n for replay attacks. Similar assumptions concerned with DoS attacks have been found in considerable achievements during the past years [19], [20]. Motivated by the mentioned researches, the inequalities in (10) and (11) are considered in Assumption 2.

Definition 1: The number of off/on transitions of replay attacks over $(0,t)$ is represented as $\mathbb{M}(t)$. The attack signal merged by F_n^1 and F_n^2 is said to satisfy the following attack frequency constraint: $\mathbb{M}(t) \leq c + \frac{t}{e_m}$, where c and e_m are positive constants.

E. Switched Event-Trigged Scheme

To save the resources of the UAV communication network, the triggering condition of the switched ETS is designed as follows:

$$\mathcal{W}_1(t) + \mathcal{W}_2(t) - \mathcal{W}_3(fh) < 0, \tag{12}$$

in which

$$\begin{aligned}
\mathcal{W}_1(t) &= \nu_i \eta_i^T(t_{\epsilon,n}^{\sigma(t)}h)\Phi_{i,\sigma(t)}\eta_i(t_{\epsilon,n}^{\sigma(t)}h),\\
\mathcal{W}_2(t) &= -\vartheta_i^T(t_{\epsilon,n}^{\sigma(t)}h)\Phi_{i,\sigma(t)}\vartheta_i(t_{\epsilon,n}^{\sigma(t)}h),\\
\mathcal{W}_3(fh) &= \kappa_i((-1)^{\sigma(t)}+1)\eta_i^T(t_{\epsilon,n}^{\sigma(t)}h+fh)\\
&\quad \times \Phi_{i,\sigma(t)}\eta_i(t_{\epsilon,n}^{\sigma(t)}h+fh),\\
\vartheta_i(t) &= \eta_i(t_{\epsilon,n}^{\sigma(t)}h) - \eta_i((t_{\epsilon,n}^{\sigma(t)}h+fh),\\
t_{\epsilon,n}^{\sigma(t)}h &= \begin{cases}\mathcal{T}_n, & \sigma(t)=1,\\ \mathcal{T}_n+S_n, & \sigma(t)=2,\end{cases}
\end{aligned}$$

where $\nu_i \in [0,1)$; κ_i is a predefined positive scalar; $\Phi_{i,\sigma(t)} > 0$ is the weighting matrix to be designed; $\sigma(t)=1$ for $t \in F_n^1$, and $\sigma(t)=2$ for $t\in F_n^2$, $n\in\mathcal{N}$; $\{t_{\epsilon,n}^1\}$ and $\{t_{\epsilon,n}^2\}$ $(\epsilon\in\mathcal{N})$ are the releasing instants in the n-th sleeping period and active period, respectively; $\eta_i(t_{\epsilon,n}^{\sigma(t)}h+fh)$ denotes the current sampling signal. The leader UAV is not triggered in this study.

Remark 5: In (12), the switched signal $\sigma(t)$ is adopted to distinguish which type of replay attacks: active or sleeping in an attack period. $\sigma(t)=1$ means that the replay attack is sleeping in intervals F_n^1, $n\in\mathcal{N}$, under this circumstance, the triggering condition turns into the representative one in [29]. When $\sigma(t)=2$, the triggering condition $\mathcal{W}_1(t)+\mathcal{W}_2(t)-\mathcal{W}_3(fh) < 0$ with $\mathcal{W}_3(fh)\geq 0$ brings larger inter-execution time, in other words, fewer data can be delivered during the active period of replay attacks. Note that the value of κ_i has influences on the data release rate. Larger κ_i leads to a lower data release rate, which will be demonstrated in Table I.

Remark 6: According to the definition of $t_{\epsilon,n}^{\sigma(t)}h$ in (12), one can get that the sampling data are compulsorily released at the right endpoint of the sleeping and active period. Then, it yields that $\sup\{t_{\epsilon,n}^1 h\} < \mathcal{T}_n + S_n$ and $\sup\{t_{\epsilon,n}^2 h\} < \mathcal{T}_{n+1}$ hold for $\epsilon, n\in\mathcal{N}$.

TABLE I
THE ATD OF FOUR UAVS FOR DIFFERENT VALUES OF κ_i

	$\kappa_i=0.02$	$\kappa_i=0.1$	$\kappa_i=0.2$
ATD of UAV 1	669	217	162
ATD of UAV 2	696	229	174
ATD of UAV 3	697	264	168
ATD of UAV 4	675	204	152

Denote $\Pi_n^1 \triangleq \sup\{\epsilon | t_{\epsilon,n}^1 h < \mathcal{T}_n + S_n\}$, $\Pi_n^2 \triangleq \sup\{\epsilon | t_{\epsilon,n}^2 h < \mathcal{T}_{n+1}\}$ and $t_{n,\Pi_n^1+1}^1 h \triangleq \mathcal{T}_n + S_n$, $t_{n,\Pi_n^2+1}^2 h \triangleq \mathcal{T}_{n+1}$. Similar analytical method adopted in [30], $[t_{\epsilon,n}^{\sigma(t)}h, t_{\epsilon,n+1}^{\sigma(t)}h), n\in\{0,1,\ldots,\Pi_n^{\sigma(t)}\}$ can be divided as $\mathbf{f}_M+1$ subintervals with $\mathbf{f}_M\in\mathcal{N}$. It follows that $[t_{\epsilon,n}^{\sigma(t)}h, t_{\epsilon,n+1}^{\sigma(t)}h) = \cup_{f=1}^{\mathbf{f}_M+1}\Gamma_{\epsilon,n,f}^{\sigma(t)}$ with $\Gamma_{\epsilon,n,f}^{\sigma(t)} \triangleq [b_{\epsilon,n}^{\sigma(t)}, b_{\epsilon,n+1}^{\sigma(t)})$, $b_{\epsilon,n}^{\sigma(t)} \triangleq t_{\epsilon,n}^{\sigma(t)}h + fh$, further, one has $\Gamma_{\epsilon,n,f}^{\sigma(t)} \in \cup_{n\in\mathcal{N}} F_n^{\sigma(t)}$.

Defining $\tau(t) = t - t_{\epsilon,n}^{\sigma(t)}h - fh$ follows that $0\leq\tau(t) < h$. Then, the event-triggered sampled state is expressed as

$$\tilde{\eta}_i(t) = \eta_i(t_{\epsilon,n}^{\sigma(t)}h) = \eta_i(t-\tau(t)) + \vartheta_i(t). \tag{13}$$

F. Observer Design

The observer for the i-th UAV is designed as follows:

$$\dot{\hat{\eta}}_i(t) = A\hat{\eta}_i(t) + Bu_{\eta i}(t) + BH_{\sigma(t)}[\bar{\eta}_i(t) - \hat{\eta}_i(t)], t\in\Gamma_{\epsilon,n,f}^{\sigma(t)}, \tag{14}$$

where $H_{\sigma(t)}$, $\sigma(t)\in\{1,2\}$ are observer gains to be designed.

Denote the observation error as $\delta_{\eta i}(t) = \eta_i(t) - \hat{\eta}_i(t)$, then, combining (8) and (14) follows that

$$\dot{\delta}_{\eta i}(t) = A\delta_{\eta i}(t) + U\tilde{d}_i(t) - BH_{\sigma(t)}[\bar{\eta}_i(t) - \hat{\eta}_i(t)], t\in\Gamma_{\epsilon,n,f}^{\sigma(t)}. \tag{15}$$

The purpose of this study is to develop observer-based formation control strategies for multi-UAV systems under replay attacks to achieve the formation by applying the proposed switched ETS such that the error system is exponentially stable.

III. MAIN RESULTS ON EVENT-TRIGGERED SMC DESIGN

A. Observer-Based Event-Triggered Sliding Mode Surface

The observer-based event-triggered sliding mode surface is developed as

$$s_i(t) = D\hat{\eta}_i(t) - \int_0^t D(A+BK_{\sigma(t)})\hat{\eta}_i(r)dr, t\in\Gamma_{\epsilon,n,f}^{\sigma(t)}, \tag{16}$$

where $K_{\sigma(t)}, \sigma(t) \in \{1, 2\}$ are SMC gains to be determined; D is a coefficient matrix, and DB is invertible.

Calculate the derivation of (16), then, letting $\dot{s}_i(t) = 0$ follows the equivalent observer-based SMC law

$$u^e_{\eta i}(t) = (K_{\sigma(t)} + H_{\sigma(t)})\hat{\eta}_i(t) - H_{\sigma(t)}\bar{\eta}_i(t), t \in \Gamma^{\sigma(t)}_{\epsilon,n,f}. \quad (17)$$

Substituting (17) into (14) yields the sliding dynamics

$$\dot{\hat{\eta}}_i(t) = (A + BK_{\sigma(t)})\hat{\eta}_i(t), t \in \Gamma^{\sigma(t)}_{\epsilon,n,f}. \quad (18)$$

Combining (15) and (18), the following overall system dynamics is derived by adopting Kronecker product:

$$\dot{\varpi}(t) = \begin{cases} \mathcal{A}_1\varpi(t) + \mathcal{B}_1\varpi(t-\tau(t)) + \mathcal{C}_1\vartheta(t) + \mathcal{U}_1\tilde{d}(t), \\ t \in \Gamma^1_{\epsilon,n,f}, \\ \mathcal{A}_2\varpi(t) + \mathcal{B}_2\varpi(t-d(t)) + \mathcal{C}_2\vartheta(t-\varepsilon) + \mathcal{U}_2\tilde{d}(t), \\ t \in \Gamma^2_{\epsilon,n,f}, \end{cases} \quad (19)$$

where $\varpi(t) \triangleq [\hat{\eta}^T(t) \quad \delta^T_\eta(t)]^T$, $\hat{\eta}(t) = \mathrm{col}_N\{\hat{\eta}_i(t)\}$, $\delta_\eta(t) = \mathrm{col}_N\{\delta_{\eta i}(t)\}$, $\vartheta(t) = \mathrm{col}_N\{\vartheta_i(t)\}$, $\vartheta(t-\varepsilon) = \mathrm{col}_N\{\vartheta_i(t-\varepsilon)\}$, $\hat{\eta}(t-\tau(t)) = \mathrm{col}_N\{\hat{\eta}_i(t-\tau(t))\}$, $\hat{\eta}(t-d(t)) = \mathrm{col}_N\{\hat{\eta}_i(t-d(t))\}$, $\tilde{d}(t) = \mathrm{col}_N\{\tilde{d}_i(t)\}$, $\tilde{A} = I_N \otimes A, \tilde{B} = I_N \otimes B, \tilde{U} = I_N \otimes U$, and

$$\mathcal{A}_l = \begin{bmatrix} \tilde{A} + \tilde{B}\tilde{K}_l & 0 \\ \tilde{B}\tilde{H}_l & \tilde{A} \end{bmatrix}, \mathcal{B}_l = \begin{bmatrix} 0 & 0 \\ -\tilde{B}\tilde{H}_l & -\tilde{B}\tilde{H}_l \end{bmatrix}, \mathcal{U}_l = \begin{bmatrix} 0 \\ \tilde{U} \end{bmatrix},$$
$$\mathcal{C}_l = \begin{bmatrix} 0 \\ -\tilde{B}\tilde{H}_l \end{bmatrix}, \tilde{K}_l = I_N \otimes K_l, \tilde{H}_l = I_N \otimes H_l, l = 1, 2.$$

Here $d(t) = \varepsilon + \tau(t-\varepsilon)$, and $0 < d(t) \le d_M$, d_M is the upper bound of $d(t)$. $\varpi(t) = \varsigma(t)$, $t \in [-d_M, 0]$. The initial state of system (19) are given by $\varpi(t) = \varsigma(t), t \in [-d_M, 0]$.

Before giving the stability analysis for the discussed system, the following lemma and definition are presented.

Lemma 1: [13] If the state trajectories of the i-th UAV ($i \in \mathbb{J}_N$) can converge to and keep on the sliding surface $s_i(t) = 0$, it is easy to obtain that the multi-UAV system with N followers and one leader achieves the desired formation.

Definition 2: The discussed system (19) is said to be exponentially stable if there is a scalar $w_1 > 0$ and a decay rate $w_2 > 0$ such that the following condition

$$\|\varpi(t)\| \le w_1 e^{-w_2 t}\|\varsigma_0\|$$

holds for all $t \ge 0$, where $\varsigma_0 = \min\{\|\varsigma_0\|_h, \|\varsigma_0\|_{d_M}\}$, $\|\varsigma_0\|_h = \sup_{-h\le v<0}\{\|\varsigma(v)\|, \|\varsigma(\dot{v})\|\}$, $\|\varsigma_0\|_{d_M} = \sup_{-d_M\le v<0}\{\|\varsigma(v)\|, \|\varsigma(\dot{v})\|\}$.

Remark 7: From the definition of $\varpi(t)$ in (19), one can know that $\varpi(t)$ consists of tracking error $\delta_\eta(t)$ and estimation error $\hat{\eta}(t)$. In case system (19) is asymptotically stable, $\delta_\eta(t) \to 0$, which means that the multi-UAV system with N followers and one leader could realize the formation tracking in accordance with Definition 2.

B. Sliding Mode Control Strategy

An observer-based event-triggered SMC strategy is proposed in this section, which can ensure the accessibility of sliding mode surface (16).

Theorem 1: Under the switched ETS (12) and observer (14), if sliding mode surface $s_i(t)$ is chosen as (16), the system trajectories could be driven onto this sliding mode surface by the controller designed as follows:

$$u_{\eta i}(t) = (K_{\sigma(t)} + H_{\sigma(t)})\hat{\eta}_i(t) - (\alpha_i + o_i(t))\mathbb{S}(s_i(t)), \quad (20)$$

in which

$$\mathbb{S}(s_i(t)) = \begin{cases} \frac{s_i(t)}{\|s_i(t)\|}, \|s_i(t)\| \ge \beta_i, \\ \frac{s_i(t)}{\beta_i}, \|s_i(t)\| < \beta_i, \end{cases} \quad o_i(t) = \|H_{\sigma(t)}\|\|\bar{\eta}_i(t)\|, t \in \Gamma^{\sigma(t)}_{\epsilon,n,f},$$

where α_i, β_i ($i \in \mathbb{J}_N$) are given positive constants.

Proof: Calculating the derivative of (16) and substituting (14), (20) into it, one has

$$\dot{s}_i(t) = DB\{u_{\eta i}(t) - (K_{\sigma(t)} + H_{\sigma(t)})\hat{\eta}_i(t) + H_{\sigma(t)}\bar{\eta}_i(t)\}. \quad (21)$$

The Lyapunov function is constructed as follows:

$$\mathcal{V}_{si}(t) = 0.5s^T_i(t)(DB)^{-1}s_i(t). \quad (22)$$

Calculate the derivation of (22), then, combining it and (20), (21) yields that

$$\begin{aligned} \dot{\mathcal{V}}_{si}(t) &= s^T_i(t)(DB)^{-1}\dot{s}_i(t) \\ &= s^T_i(t)\big[-(\alpha_i + o_i(t))\mathbb{S}(s_i(t)) + H_{\sigma(t)}\bar{\eta}_i(t)\big]. \end{aligned} \quad (23)$$

When $\|s_i(t)\| \ge \beta_i$, based on controller (20) with $\sigma(t) = 1$ for $t \in \Gamma^{\sigma(t)}_{\epsilon,n,f}$, one can get

$$\begin{aligned} \dot{\mathcal{V}}_{si}(t) &\le -(\alpha_i + o_i(t))\|s_i(t)\| + \|H_1\|\|\bar{\eta}_i(t)\|\|s_i(t)\| \\ &= -\alpha_i\|s_i(t)\|; \end{aligned} \quad (24)$$

based on controller (20) with $\sigma(t) = 2$ for $t \in \Gamma^{\sigma(t)}_{\epsilon,n,f}$, it is easy to obtain that

$$\begin{aligned} \dot{\mathcal{V}}_{si}(t) &\le -(\alpha_i + o_i(t))\|s_i(t)\| + \|H_2\|\|\bar{\eta}_i(t)\|\|s_i(t)\| \\ &= -\alpha_i\|s_i(t)\|. \end{aligned} \quad (25)$$

When $\|s_i(t)\| < \beta_i$, with the similar analytical method, it follows from controller (20) that

$$\begin{aligned} \dot{\mathcal{V}}_{si}(t) &\le -(\alpha_i + o_i(t))\frac{\|s(t)\|^2}{\beta_i} + \|H_{\sigma(t)}\|\|\bar{\eta}_i(t)\|\|s_i(t)\| \\ &= \frac{-\alpha_i\|s_i(t)\|^2}{\beta_i} + \frac{o_i(t)}{\beta_i}(\|s_i(t)\|\beta_i + \|s_i(t)\|^2) \end{aligned} \quad (26)$$

holds for $t \in \Gamma^1_{\epsilon,n,f} \cup \Gamma^2_{\epsilon,n,f}$. Further, it can be concluded that for $t \geq b^1_{0,0}h$, there exists a proper α_i such that $\dot{\mathcal{V}}_{si}(t) < 0$, $s_i(t) \neq 0$, which indicates that every UAV could arrive at the sliding surface and subsequently maintain on it. As a result, it follows from Lemma 1 that the formation tracking issue is turned into a SMC problem. That ends the proof. ■

C. Performance Analysis

The accessibility of sliding mode surface (16) has been discussed in Theorem 1. In the following Theorem 2, we will present the stability analysis of the system on the sliding mode surface. Besides, sufficient conditions of the multi-UAV system to achieve the desired formation will be acquired as well. Based on this, we can obtain controller gains and observer gains.

Theorem 2:

For known scalars $\nu_i \in (0,1)$, $\mathcal{T}_M$, $\mathcal{T}_m$, e_m, h, ϱ_l, b_{lk}, system (19) is exponentially stable if there exist positive definite matrices $\tilde{P}_{lk}$, Q_{lk}, R_{lk}, Φ_{il} and matrices $\tilde{Y}_{lk}$ $(l,k \in \{1,2\}$, $i \in \mathbb{J}_N)$ such that the following linear matrix inequalities hold:

$$\begin{bmatrix} -\varrho_2 \tilde{P}_{2\,k} & * \\ \tilde{P}_{1\,k} & -\tilde{P}_{1\,k} \end{bmatrix} \leq 0, \tag{27}$$

$$\begin{bmatrix} -\delta_0 \varrho_1 \tilde{P}_{1\,k} & * \\ \tilde{P}_{2\,k} & -\tilde{P}_{2\,k} \end{bmatrix} \leq 0, \tag{28}$$

$$\begin{bmatrix} -\varrho_l Q_{lk} & * \\ Q_{3-l,k} & -Q_{3-l,k} \end{bmatrix} \leq 0, \tag{29}$$

$$\begin{bmatrix} -\varrho_l R_{lk} & * \\ R_{3-l,k} & -R_{3-l,k} \end{bmatrix} \leq 0, \tag{30}$$

$$\begin{aligned} \mu = (2\delta_1 \mathcal{T}_m - 2(\delta_1 h + \delta_2 d_M) \\ - 2\delta_2 \mathcal{T}_M - \ln(\varrho_1 \varrho_2))/e_m > 0, \end{aligned} \tag{31}$$

$$\bar{\Pi}_l = \begin{bmatrix} \bar{\Gamma}^l_1 & * \\ \bar{\Gamma}^l_2 & \bar{\Gamma}^l_3 \end{bmatrix} < 0, \tag{32}$$

where

$$\bar{\Gamma}^l_1 = \begin{bmatrix} \Psi^l_{11} & * & * & * & * & * & * & * \\ \Psi^l_{21} & \Psi^l_{22} & * & * & * & * & * & * \\ \Psi^l_{31} & \Psi^l_{32} & \Psi^l_{33} & * & * & * & * & * \\ 0 & \Psi^l_{42} & \Psi^l_{43} & \Psi^l_{44} & * & * & * & * \\ \Psi^l_{51} & 0 & \Psi^l_{53} & 0 & \Psi^l_{55} & * & * & * \\ 0 & \Psi^l_{62} & 0 & \Psi^l_{64} & 0 & \Psi^l_{66} & * & * \\ 0 & \Psi^l_{72} & 0 & 0 & 0 & 0 & -\Phi_l & * \\ 0 & \Psi^l_{82} & 0 & 0 & 0 & 0 & 0 & -I \end{bmatrix},$$

$$\bar{\Gamma}^l_2 = \begin{bmatrix} h\Psi^l_{91} \\ h\Psi^l_{101} \end{bmatrix},$$

$$\bar{\Gamma}^l_3 = \mathrm{diag}\{-2b_{l1}\tilde{P}_{l1} + b^2_{l1}R_{l1}, -2b_{l2}\tilde{P}_{l1} + b^2_{l2}R_{l2}\},$$

$$\begin{aligned} \Psi^l_{11} &= \mathrm{sym}\{\tilde{P}_{l1}\tilde{A} + \tilde{Y}_{l1}\} + Q_{l1} + 2(-1)^l \delta_l \tilde{P}_{l1} \\ &\quad - r_l R_{l1} + \tilde{F}^T \tilde{F}, \\ \Psi^l_{22} &= \mathrm{sym}\{\tilde{P}_{l1}\tilde{A}\} + Q_{l2} + 2(-1)^l \delta_l \tilde{P}_{l1} - r_l R_{l2} + \tilde{F}^T \tilde{F}, \\ \Psi^l_{21} &= Y_{l2} + \tilde{F}^T \tilde{F}, \Psi^l_{31} = r_l(R_{l1} + M_{l1}), \Psi^l_{32} = -Y^T_{l2}, \\ \Psi^l_{33} &= r_l(-2R_{l1} - M_{l1} - M^T_{l1}) + \nu\Phi_l, \Psi^l_{42} = -Y^T_{l2} + \Psi^l_{64}, \\ \Psi^l_{43} &= \nu\Phi_l, \Psi^l_{44} = r_l(-2R_{l2} - M_{l2} - M^T_{l2}) + \nu\Phi_l, \\ \nu &= \nu_0 \otimes I_{2q}, \nu_0 = \mathrm{diag}\{\nu_1, \nu_2, \ldots, \nu_N\}, \\ \Phi_l &= \mathrm{diag}\{\Phi_{1\,l}, \Phi_{2\,l}, \ldots, \Phi_{Nl}\}, \\ \Psi^l_{51} &= -r_l M_{l1}, \Psi^l_{53} = \Psi^l_{31}, \Psi^1_{55} = -r_1(R_{l1} + Q_{l1}), \\ \Psi^2_{55} &= -r_2 R_{l1} - r_3 Q_{l1}, \Psi^l_{62} = -r_l M_{l2}, \\ \Psi^l_{64} &= r_l(R_{l2} + M_{l2}), \Psi^1_{66} = -r_1(R_{l2} + Q_{l2}), \\ \Psi^2_{66} &= -r_2 R_{l2} - r_3 Q_{l2}, \Psi^l_{72} = -\tilde{Y}^T_{l2}, \\ \Psi^l_{82} &= \tilde{U}^T \tilde{P}_{l1}, r_1 = e^{-2\delta_1 h}, r_2 = 1, r_3 = e^{2\delta_2 d_M}, \\ \Psi^l_{91} &= \begin{bmatrix} \tilde{P}_{l1}\tilde{A} + \tilde{Y}_{l1} & 0_{1\times 7} \end{bmatrix}, \\ \Psi^l_{101} &= \begin{bmatrix} \Psi^l_{111} & \Psi^l_{121} \end{bmatrix}, \Psi^l_{111} = \begin{bmatrix} \tilde{Y}_{l2} & \tilde{P}_{l1}\tilde{A} \end{bmatrix}, \\ \Psi^l_{121} &= \begin{bmatrix} -\tilde{Y}_{l2} & -\tilde{Y}_{l2} & 0 & 0 & -\tilde{Y}_{l2} & \tilde{P}_{l1}\tilde{U} \end{bmatrix}. \end{aligned}$$

Furthermore, controller gains K_l and observer gains H_l are designed as

$$K_l = B^T P^{-1}_{l1} Y_{l1}, H_l = B^T P^{-1}_{l1} Y_{l2}, l = \{1,2\}. \tag{33}$$

Proof: Choose the following Lyapunov function for system (19):

$$\begin{aligned} \mathcal{V}_l(\varpi(t)) &= \varpi^T(t)\tilde{P}_l\varpi(t) + \int_{t-\varsigma_l}^t \rho_l \varpi^T(r) G^T_1 Q_{1\,l} G_1 \varpi(r) dr \\ &\quad + \int_{t-\varsigma_l}^t \rho_l \varpi^T(r) G^T_2 Q_{2\,l} G_2 \varpi(r) dr \\ &\quad + \varsigma_l \int_{-\varsigma_l}^0 \int_{t+v}^t \rho_l \dot{\varpi}^T(r) G^T_1 R_{1\,l} G_1 \dot{\varpi}(r) dr dv \\ &\quad + \varsigma_l \int_{-\varsigma_l}^0 \int_{t+v}^t \rho_l \dot{\varpi}^T(r) G^T_2 R_{2\,l} G_2 \dot{\varpi}(r) dr dv, \end{aligned} \tag{34}$$

where $\tilde{P}_l = \mathrm{diag}\{\tilde{P}_{l1}, \tilde{P}_{l1}\}$, $\tilde{P}_{l1} = I_N \otimes P_{l1}$; $\rho_l \triangleq e^{2(-1)^l \delta_l (t-s)}$, and scalar $\delta_l > 0$. $l = 1$ for $t \in \Gamma^1_{\epsilon,n,f}$; $l = 2$ for $t \in \Gamma^2_{\epsilon,n,f}$; $\varsigma_1 = h$, $\varsigma_2 = d_M$; and $G_1 = [I_{qN} \;\; 0_{qN}]$, $G_2 = [0_{qN} \;\; I_{qN}]$.

In the following, two situations are considered for $t \in \Gamma^1_{\epsilon,n,f}$ and $t \in \Gamma^2_{\epsilon,n,f}$, respectively.

Firstly, when $t \in \Gamma^1_{\epsilon,n,f}$, namely, $t \in [b^1_{\epsilon,n}, b^1_{\epsilon,n+1})$, calculate the derivation of (34), then, we can get

$$\begin{aligned} \dot{\mathcal{V}}_1(\varpi(t)) &= 2\varpi^T(t)\tilde{P}_1\dot{\varpi}(t) + \varpi^T(t) G^T_1 Q_{11} G_1 \varpi(t) \\ &\quad + \varpi^T(t) G^T_2 Q_{21} G_2 \varpi(t) - 2\delta_1 \mathcal{V}_1(\varpi(t)) \\ &\quad - e^{2\delta_1 h} \varpi^T(t-h) G^T_1 Q_{11} G_1 \varpi(t-h) \\ &\quad - e^{2\delta_1 h} \varpi^T(t-h) G^T_2 Q_{21} G_2 \varpi(t-h) \\ &\quad - 2\delta_1 \tilde{P}_1 + h^2 \dot{\varpi}^T(t) G^T_1 R_{11} G_1 \dot{\varpi}(t) \\ &\quad + h^2 \dot{\varpi}^T(t) G^T_2 R_{21} G_2 \dot{\varpi}(t) \\ &\quad - h \int_{t-h}^t e^{-2\delta_1 h} \dot{\varpi}^T G^T_1(r) R_{11} G_1 \dot{\varpi}(r) dr \\ &\quad - h \int_{t-h}^t e^{-2\delta_1 h} \dot{\varpi}^T(r) G^T_2 R_{21} G_2 \dot{\varpi}(r) dr, \end{aligned} \tag{35}$$

Due to the existence of nonlinearities, one has

$$\varpi^T(t)G_3^T\tilde{F}^T\tilde{F}G_3\varpi(t) - \tilde{d}^T(t)\tilde{d}(t) \geq 0, \tag{36}$$

where $G_3 = [\, I_{2N} \quad I_{2N} \,]$.

From (12), it yields that

$$\begin{aligned}\nu[G_3\varpi(t-\tau(t))]^T\Phi_1 G_3\varpi(t-\tau(t))\\ - \vartheta^T(t)\Phi_1\vartheta(t) \,<\, 0.\end{aligned} \tag{37}$$

Combining (35)–(37) and utilizing Jensen's inequality [31] follow that

$$\dot{\mathcal{V}}_1(\varpi(t)) + 2\delta_1\mathcal{V}_1(\varpi(t)) \leq \chi_1^T(t)\Big[\Gamma_1^1 - \Gamma_2^1(\Gamma_3^1)^{-1}\Gamma_2^1\Big]\chi_1(t), \tag{38}$$

where $\chi_1(t) = [\varpi^T(t), \varpi^T(t-\tau(t)), \varpi^T(t-h), \vartheta^T(t), \quad \tilde{d}^T(t)]^T$, and

$$\Gamma_1^1 = \begin{bmatrix} \Lambda_{11}^1 & * & * & * & * \\ \Lambda_{21}^1 & \Lambda_{22}^1 & * & * & * \\ \Lambda_{31}^1 & \Lambda_{32}^1 & \Lambda_{33}^1 & * & * \\ \Lambda_{41}^1 & 0 & 0 & -\Phi_1 & * \\ \Lambda_{51}^1 & 0 & 0 & 0 & -\mathbf{r}^2 I \end{bmatrix},$$

$$\Gamma_2^1 = \begin{bmatrix} hG_1\tilde{P}_1\Lambda_{61}^1 \\ hG_2\tilde{P}_1\Lambda_{61}^1 \end{bmatrix},$$

$$\begin{aligned}
\Gamma_3^1 &= \mathrm{diag}\{-(G_1\tilde{P}_1)^T R_{11}^{-1} G_1\tilde{P}_1, -(G_2\tilde{P}_1)^T R_{12}^{-1} G_2\tilde{P}_1\},\\
\Lambda_{11}^1 &= \mathrm{sym}\{\tilde{P}_1\mathcal{A}_1\} + G_1^T Q_{11} G_1 + G_2^T Q_{12} G_2 + 2(-1)^1\delta_1\tilde{P}_1\\
&\quad - r_1 G_1^T R_{11} G_1 - r_1 G_2^T R_{12} G_2 + G_3^T\tilde{F}^T\tilde{F}G_3,\\
\Lambda_{22}^1 &= r_1 G_1^T(-2R_{11} - M_{11} - M_{11}^T)G_1 + G_3^T\nu\Phi_1 G_3\\
&\quad + r_1 G_2^T(-2R_{12} - M_{12} - M_{12}^T)G_2,\\
\Lambda_{31}^1 &= -r_1 G_1^T M_{11} G_1 - r_1 G_2^T M_{12} G_2, \Lambda_{21}^1 = \mathcal{B}_1^T\tilde{P}_1 + \Lambda_{32}^1,\\
\Lambda_{32}^1 &= r_1 G_1^T(R_{11} + M_{11})G_1 + r_1 G_2^T(R_{12} + M_{12})G_2,\\
\Lambda_{33}^1 &= -r_1 G_1^T(Q_{11} + R_{11})G_1 - r_1 G_2^T(Q_{12} + R_{12})G_2,\\
&\quad - r_3 G_2^T R_{22} G_2, r_1 = e^{-2\delta_1 h}, r_2 = 1, r_3 = e^{2\delta_2 d_M},\\
\Lambda_{41}^1 &= \mathcal{C}_1^T\tilde{P}_1, \Lambda_{51}^1 = \mathcal{U}_1^T\tilde{P}_1, \Lambda_{61}^1 = [\, \mathcal{A}_1 \quad \mathcal{B}_1 \quad 0 \quad \mathcal{C}_1 \quad \mathcal{U}_1 \,].
\end{aligned}$$

Applying Schur's complement to (38) yields that $\Pi_1 \,<\, 0 (\Pi_1 = \begin{bmatrix} \Gamma_1^1 & * \\ \Gamma_2^1 & \Gamma_3^1 \end{bmatrix})$ is the sufficient condition to guarantee the following inequality holds:

$$\dot{\mathcal{V}}_1(\varpi(t)) + 2\delta_1\mathcal{V}_1(\varpi(t)) \,<\, 0. \tag{39}$$

Integrating both sides of (39) for $t \in [b_{\epsilon,n,f}^1, b_{\epsilon,n+1,a}^1)$, one can get

$$\mathcal{V}_1(\varpi(t)) \,<\, e^{-2\delta_1(t-b_{\epsilon,n,f}^1)}\mathcal{V}_1(b_{\epsilon,n,f}^1). \tag{40}$$

Seconly, when $t \in \Gamma_{\epsilon,n,f}^2$, namely $t \in [b_{\epsilon,n}^2, b_{\epsilon,n+1}^2)$, applying the similar analytical method as above, it is easy to obtain $\dot{\mathcal{V}}_2(\varpi(t)) - 2\delta_2\mathcal{V}_2(\varpi(t)) \,<\, 0$. Integrating its both sides for $t \in [b_{\epsilon,n,f}^2, b_{\epsilon,n+1,a}^2)$ yields that

$$\mathcal{V}_2(\varpi(t)) \,<\, e^{2\delta_2(t-b_{\epsilon,n,f}^2)}\mathcal{V}_2(b_{\epsilon,n,f}^2). \tag{41}$$

Moreover, according to sufficient conditions: $\tilde{P}_1 \leq \varrho_2\tilde{P}_2$, $\tilde{P}_2 \leq \delta_0\varrho_1\tilde{P}_2, \delta_0 = e^{2(\delta_1 h + \delta_2 d_M)}$, the following inequalities are acquired:

$$\begin{cases} \mathcal{V}_1(b_{\epsilon,n,f}^1) \;\,<\, \varrho_2\mathcal{V}_2(b_{\epsilon,n,f}^{1-}), \\ \mathcal{V}_2(b_{\epsilon,n,f}^2) \,<\, \delta_0\varrho_1\mathcal{V}_1(b_{\epsilon,n,f}^{2-}). \end{cases} \tag{42}$$

If $t \in [\mathcal{T}_n + S_n, \mathcal{T}_{n+1})$, based on (42), we have $\mathcal{V}(\varpi(t)) \leq e^{2\delta_2(t-t_{0,n}^2)}\mathcal{V}_2(t_{0,n}^2 h)$, then, $\mathcal{V}_2(t_{0,n}^2 h) \leq \delta_0\varrho_1\mathcal{V}_1(t_{0,n}^{2-}h)$ and $\mathcal{V}_1(t_{0,n}^{2-}h) \leq e^{-2\delta_1(t_{0,n}^2 h - t_{0,n}^1 h)}\mathcal{V}_1(t_{0,n}^1 h)$ are derived because $t_{0,n}^{2-}h \in [t_{0,n}^1 h, t_{0,n}^2 h)$. Reiterating this process follows that

$$\mathcal{V}(\varpi(t)) \leq e^{-\mu t}\mathcal{V}_1(0), \tag{43}$$

where $\mu = (2\delta_1\mathcal{T}_m - 2(\delta_1 h + \delta_2 d_M) - 2\delta_2\mathcal{T}_M - \ln(\varrho_1\varrho_2))/e_m$.

If $t \in [\mathcal{T}_n, \mathcal{T}_n + S_n)$, conducting the similar operation as above yields that

$$\begin{aligned}\mathcal{V}(\varpi(t)) &\leq \delta_0^n\varrho_1^n\varrho_2^n e^{2\delta_2\mathcal{T}_M}e^{-2(n+1)\delta_1\mathcal{T}_m}\mathcal{V}_1(0)\\ &\leq e^{-\mu t}\mathcal{V}_1(0).\end{aligned} \tag{44}$$

According to the definition of $\mathcal{V}(\varpi(t))$, one has

$$\lambda_1\|\varpi(t)\|^2 \leq \mathcal{V}(0) \leq \gamma\|\varsigma(0)\|^2, \tag{45}$$

where $\lambda_1 = \min\{\lambda_{\mathrm{m}}(\tilde{P}_l)\}$, $l = \{1,2\}$, $\|\varsigma(0)\|^2 = \min\{\|\varsigma(0)\|_h^2, \|\varsigma(0)\|_{d_M}^2\}$, $\gamma = \min\{\gamma_1, \gamma_2\}$, $\gamma_1 = \max\{\lambda_{\mathrm{M}}(\tilde{P}_1)\} + h\max\{\lambda_{\mathrm{M}}(Q_{k1})\} + \frac{h^2}{2}\max\{\lambda_{\mathrm{M}}(R_{11} + R_{21})\}$, $\gamma_2 = \max\{\lambda_{\mathrm{M}}(\tilde{P}_2)\} + d_M\max\{\lambda_{\mathrm{M}}(Q_{k2})\} + \frac{d_M^2}{2}\max\{\lambda_{\mathrm{M}}(R_{12} + R_{22})\}$, $k = \{1,2\}$.

Combining (43)–(45) follows that

$$\|\varpi(t)\| \leq \sqrt{\gamma}e^{-\frac{\mu}{2}t}\|\varsigma(0)\|, \tag{46}$$

In the light of the aforementioned analysis and discussion, one can conclude from Definition 2 that system (19) is exponentially stable.

Recall the fact that the matrix $\tilde{P}_l$ is in the form $\tilde{P}_l = \begin{bmatrix} \tilde{P}_{l1} & 0 \\ 0 & \tilde{P}_{l1} \end{bmatrix}$, where $\tilde{P}_{l1} = I_N \otimes P_{l1}, l = \{1,2\}$. Invoking them into Γ_3^l yields $\Gamma_3^l = \mathrm{diag}\{-\tilde{P}_{l1}R_{l1}^{-1}\tilde{P}_{l1}, -\tilde{P}_{l1}R_{l2}^{-1}\tilde{P}_{l1}\}$.

Owing to $(R_{l1} - b_{l1}^{-1}\tilde{P}_{l1})R_{l1}(\bar{R}_{l1} - b_{l1}^{-1}\tilde{P}_{l1}) \geq 0$, we have $-\tilde{P}_{l1}R_{l1}^{-1}\tilde{P}_{l1} \leq -2b_{l1}\tilde{P}_{l1} + b_{l1}^2 R_{l1}$. Similarly, it follows that

$-\tilde{P}_{l1}R_{l2}^{-1}\tilde{P}_{l1} \leq -2b_{l2}\tilde{P}_{l1} + b_{l2}^2 R_{l2}$. Then, we can get $\Gamma_3^l = \mathrm{diag}\{-2b_{l1}\tilde{P}_{l1} + b_{l1}^2 R_{l1}, -2b_{l2}\tilde{P}_{l1} + b_{l2}^2 R_{l2}\}, l = \{1, 2\}$.

Defining $Y_{l1} = P_{l1}BK_l$, $Y_{l2} = P_{l1}BH_l$ yields (32). By applying Schur's complement, one has (27)–(30). Moreover, the parameters of both the controller and the observer can be obtained according to (33). That ends the proof. ■

IV. Illustrative Example

To evaluate the performance of the proposed approach, a simulation example is given in this section. Consider a multi-UAV system consisting of four follower UAVs and one leader. Fig. 5 presents the directed communication topology of the multi-UAV system, from which one can obtain $w_{12} = 1, w_{23} = 1, w_{34} = 1, a_1 = 1, a_4 = 1$.

The design of the formation tracking controller in three-axis directions (namely, $q = 3$) is considered in this simulation. In the case of $q = 3$, $x_i(t)$ and $u_i(t)$ of the i-th UAV ($i \in \{1, 2, 3, 4\} \triangleq \mathbb{J}_4$) can be rewritten as $x_i(t) = [\zeta_{iX}(t), v_{iX}(t), \zeta_{iY}(t), v_{iY}(t), \zeta_{iZ}(t), v_{iZ}(t)]^T$ and $u_i(t) = [u_{iX}(t), u_{iY}(t), u_{iZ}(t)]^T$, respectively. It is supposed that the time-varying formation for all followers is a time-varying square formation from the perspective of the Y-Z plane, and retains the rotation around the leader UAV (its dynamic is $[20t, 5t, 5t]^T$). The corresponding formation vector is $g_i(t) =$

$$\begin{bmatrix} 0 \\ 0 \\ 10t\cos\left(wt + (i-1)\frac{\pi}{2}\right) \\ 10\cos\left(wt + (i-1)\frac{\pi}{2}\right) - 10\ wt\sin\left(wt + (i-1)\frac{\pi}{2}\right) \\ 10t\sin\left(wt + (i-1)\frac{\pi}{2}\right) \\ 10\sin\left(wt + (i-1)\frac{\pi}{2}\right) + 10\ wt\cos\left(wt + (i-1)\frac{\pi}{2}\right) \end{bmatrix}, \quad i \in$$

$\mathbb{J}_4$ with $w = 0.314$ rad/s.

Set $h = 0.01$s, $\mathcal{T}_m = 400\ h$, $\mathcal{T}_M = 81\ h$, $\varepsilon = 81\ h$, $d_M = h + \varepsilon = 82\ h$, $\varrho_1 = \varrho_2 = 1.08$, $\delta_1 = 0.35$, $\delta_2 = 0.75$ such that inequality (31) holds. The nonlinear function $\tilde{d}_i(t)$ satisfies inequality $\|\tilde{d}_i(t)\|_2 \leq \|\tilde{F}\eta_i(t)\|_2$ with $\tilde{F} = \mathrm{diag}\{0.2, 0.3, 0.35, 0.25, 0.15, 0.2\}$. Let $\nu_1 = 0.02$, $\nu_2 = 0.15$, $\nu_3 = 0.016$, $\nu_4 = 0.023$, $\kappa_i = 0.2$ $(i \in \mathbb{J}_4)$, $b_{11} = b_{12} = 0.1$, $b_{21} = b_{22} = 0.1$. From Theorem 2, the follwing parameters can be obtained.

$$K_l = I_3 \otimes K_{l0}, H_l = I_3 \otimes H_{l0}, l \in \{1, 2\},$$
$$K_{10} = [-1.6739 \quad -6.0007], K_{20} = [-1.6047 \quad -7.0868],$$
$$H_{10} = [0.7684 \quad 2.5877], H_{20} = [0.5447 \quad 1.9035],$$
$$\Phi_{i1} = (I_3 \otimes \Phi_{i10}), \Phi_{i2} = (I_3 \otimes \Phi_{i20}), i \in \mathbb{J}_4,$$
$$\Phi_{110} = \begin{bmatrix} 8.5237 & 0.647 \\ 0.6473 & 8.225 \end{bmatrix}, \ \Phi_{210} = \begin{bmatrix} 8.6302 & 0.6928 \\ 0.6928 & 8.3114 \end{bmatrix},$$
$$\Phi_{310} = \begin{bmatrix} 8.6917 & 0.7270 \\ 0.7270 & 8.3577 \end{bmatrix}, \Phi_{410} = \begin{bmatrix} 8.5532 & 0.6687 \\ 0.6687 & 8.2449 \end{bmatrix},$$
$$\Phi_{120} = \begin{bmatrix} 7.7568 & 0.2090 \\ 0.2090 & 7.5708 \end{bmatrix}, \Phi_{220} = \begin{bmatrix} 7.8967 & 0.2191 \\ 0.2191 & 7.6980 \end{bmatrix},$$
$$\Phi_{320} = \begin{bmatrix} 7.9842 & 0.2276 \\ 0.2276 & 7.7749 \end{bmatrix}, \Phi_{420} = \begin{bmatrix} 7.8031 & 0.2152 \\ 0.2152 & 7.6100 \end{bmatrix}.$$

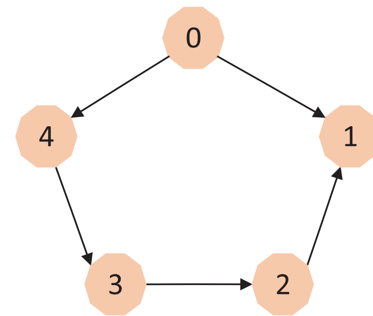

Fig. 5. Communication topology of the multi-UAV system.

The initial parameters are given as follows: the position of four follower UAVs $\zeta_{10} = [10, 11, 9]^T$, $\zeta_{20} = [5, 6, 7]^T$, $\zeta_{30} = [6.5, 8, 9.5]^T$, and $\zeta_{40} = [3, 4, 5.5]^T$. Based on the derived parameters above, one has obtained Figs. 6–11.

The responses of tracking errors $\eta(t)$ and tracking position errors of four UAVs are presented in Fig. 6, from which we can see that the UAV formation system with replay attacks is asymptotically stable. At this time, four UAVs achieve their own corresponding desired position and formulate this formation. To display the formation more distinctly, Fig. 7 shows the trajectories of the formation tracking for every UAV, in which position snapshots at instants 20, 50 s are presented for the leader and four UAVs.

The third subgraph in Fig. 6 exhibits the responses of observation errors $\delta_{\eta i}(t)$ $(i \in \mathbb{J}_4)$ between tracking errors and their estimations. Fig. 8 plots the responses of the switching function $s(t)$ of four UAVs. This indicates that utilizing such observers brings the satisfactory performance of multi-UAV systems under replay attacks, and every UAV could converge to the sliding mode surface and keep on it. Fig. 9 displays the responses of formation control inputs for the i-th UAV, $i \in \mathbb{J}_4$.

Fig. 10 reveals the responses of replay attack signal with $\mathcal{T}_m = 400\ h$, $\mathcal{T}_M = 81\ h$. From Fig. 10, it can be seen that grey areas denote the intervals without replay attacks; red areas represent the intervals when the replay attack signal is active, under this circumstance, the normally transmitted packets are replaced by these during a certain period in the past.

To express the effect of the proposed switched ETS, triggering instants and releasing intervals of the i-th UAV, $i \in \mathbb{J}_4$ are shown in Fig. 10. Under the switched ETS, the network bandwidth load is alleviated observably because 162 sampled signals of the 1-th UAV are transmitted to its neighbors and its controller side in [0, 50]s with 5000 data. Comparative work is conducted by setting different values of κ_i in the ETS (12). The amount of transmitted data (ATD) of four UAVs under different values of κ_i is recorded in Table I. From this table, one can see that fewer sampled signals are delivered with the increase of κ_i, which is consistent with the analysis of the switched ETS in Remark 5.

To further demonstrate the superiority of the proposed switched ETS, a comparison of the ATD for some existing communication mechanisms is displayed in Fig. 11 under the same condition and parameters as above. From Figs. 10–11, one can observe that the ATD under the switched ETS proposed in this research is obviously less than those under other communication mechanisms, including the time-triggered

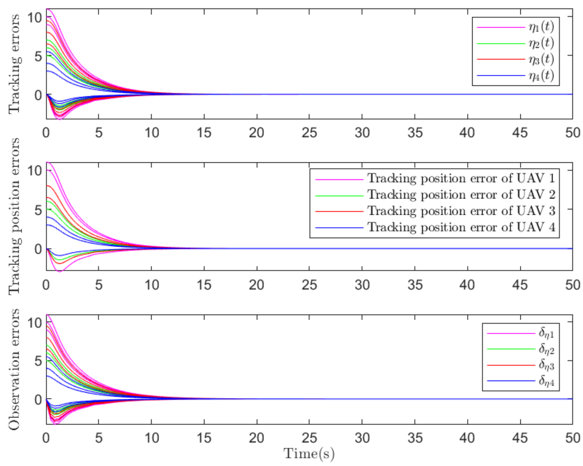

Fig. 6. Tracking errors, tracking position errors and observation errors of four UAVs.

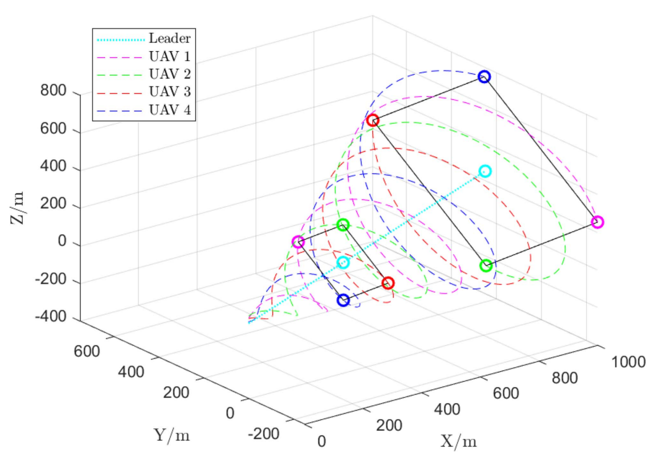

Fig. 7. Position trajectories of the leader and four UAVs, and position snapshots at $t = 20, 50$ s.

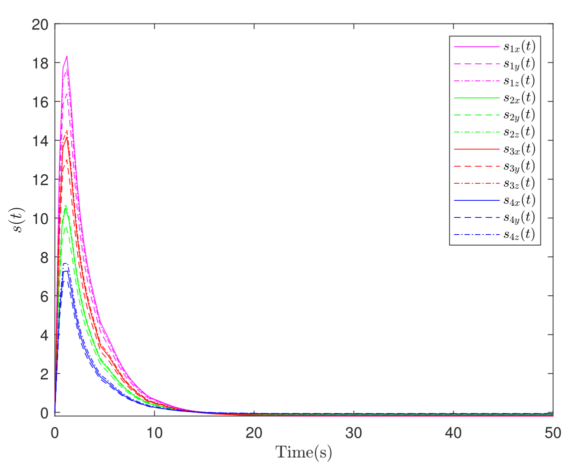

Fig. 8. Switching function $s(t)$ of four UAVs.

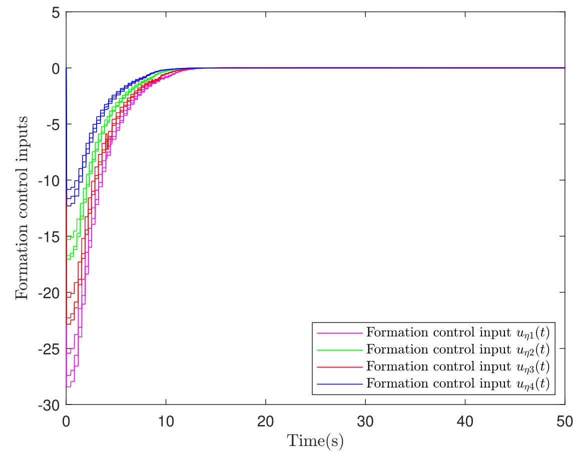

Fig. 9. Formation control inputs of four UAVs.

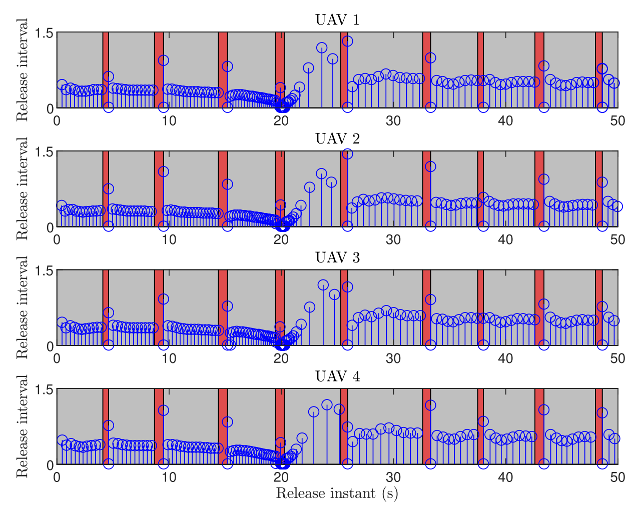

Fig. 10. Replay attack signal, and release instants of four UAVs.

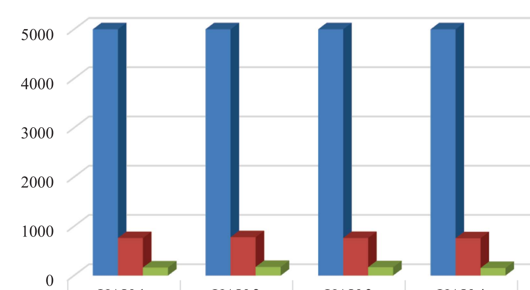

	UAV 1	UAV 2	UAV 3	UAV 4
TTS	5000	5000	5000	5000
ETS in [28]	761	778	762	757
This study	162	174	168	152

Fig. 11. Comparisons of the ATD for some existing communication mechanisms.

scheme (TTS) and the ETS in [28]. This implies that our proposed switched ETS can lessen the bandwidth overhead of the UAV communication network.

In addition, to show the advantage of the proposed observer-based sliding mode control, we present tracking errors $\eta(t)$ and tracking position errors of four UAVs under the control method in [28], which are shown in Fig. 12. Compared Fig. 12 with Fig. 6, one can conclude that the proposed observer-based sliding mode control method brings better performance of the multi-UAV system with nonlinear inputs under replay attacks than the one in [28].

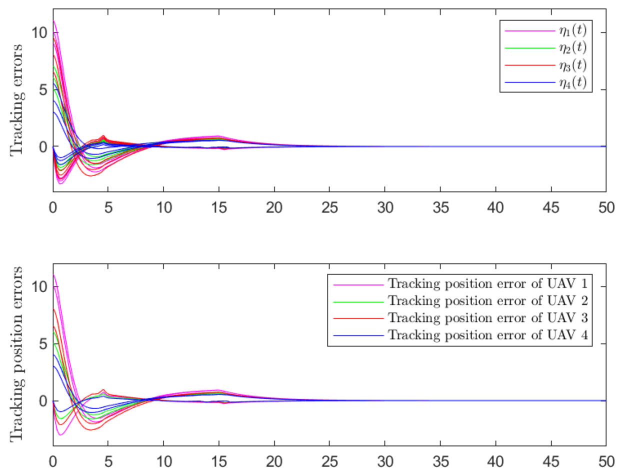

Fig. 12. Tracking errors and tracking position errors of four UAVs under the control method in [28].

V. Conclusion

In this article, the formation tracking issue of multi-UAVs under replay attacks has been studied by using an observer-based event-triggered SMC approach. First, a novel attack model is built to describe replay attacks. Then, a switched ETS is developed, which can invoke appropriate communication schemes for different attack states. Under this switched ETS, the amount of transmitted data is greatly decreased without compromising the desired system performance, thereby saving network resources. In view of the SMC theory, observer-based event-triggered formation tracking control laws are proposed for multi-UAV systems with replay attacks by adopting interactive information from neighbors. Sufficient conditions are presented for the multi-UAV system to achieve the formation via a Lyapunov stability approach. At last, a simulation example with multiple UAVs is performed, where the validity of the developed formation control laws is demonstrated. In the future, we will focus on the problem of containment formation control for multi-UAV systems with multiple leaders, along with the detection and defense of cyber-attacks.

References

[1] F. De Vivo, M. Battipede, and E. Johnson, "Infra-red line camera data-driven edge detector in UAV forest fire monitoring," *Aerosp. Sci. Technol.*, vol. 111, Apr. 2021, Art. no. 106574.

[2] J. Han, Y. Xu, L. Di, and Y. Chen, "Low-cost multi-UAV technologies for contour mapping of nuclear radiation field," *J. Intell. Rob. Syst.*, vol. 70, no. 1, pp. 401–410, Apr. 2013.

[3] J. Seo, Y. Kim, S. Kim, and A. Tsourdos, "Collision avoidance strategies for unmanned aerial vehicles in formation flight," *IEEE Trans. Aerosp. Electron. Syst.*, vol. 53, no. 6, pp. 2718–2734, Dec. 2017.

[4] W. Zhao, H. Liu, and F. L. Lewis, "Robust formation control for cooperative underactuated quadrotors via reinforcement learning," *IEEE Trans. Neural Netw. Learn. Syst.*, vol. 32, no. 10, pp. 4577–4587, Oct. 2021.

[5] J. Zhang, J. Yan, and P. Zhang, "Multi-UAV formation control based on a novel back-stepping approach," *IEEE Trans. Veh. Technol.*, vol. 69, no. 3, pp. 2437–2448, Mar. 2020.

[6] H. Liu, Y. Tian, F. L. Lewis, Y. Wan, and K. P. Valavanis, "Robust formation tracking control for multiple quadrotors under aggressive maneuvers," *Automatica*, vol. 105, pp. 179–185, Jul. 2019.

[7] V. P. Tran, F. Santoso, M. A. Garratt, and S. G. Anavatti, "Distributed artificial neural networks-based adaptive strictly negative imaginary formation controllers for unmanned aerial vehicles in time-varying environments," *IEEE Trans. Ind. Inf.*, vol. 17, no. 6, pp. 3910–3919, Jun. 2021.

[8] I. Bayezit and B. Fidan, "Distributed cohesive motion control of flight vehicle formations," *IEEE Trans. Ind. Electron.*, vol. 60, no. 12, pp. 5763–5772, Dec. 2013.

[9] X. Dong, Y. Li, C. Lu, G. Hu, Q. Li, and Z. Ren, "Time-varying formation tracking for UAV swarm systems with switching directed topologies," *IEEE Trans. Neural Netw. Learn. Syst.*, vol. 30, no. 12, pp. 3674–3685, Dec. 2019.

[10] H. Liu, Y. Wang, F. L. Lewis, and K. P. Valavanis, "Robust formation tracking control for multiple quadrotors subject to switching topologies," *IEEE Trans. Control Netw. Syst.*, vol. 7, no. 3, pp. 1319–1329, Sep. 2020.

[11] Y. Wang, D. Wang, and S. Zhu, "Cooperative moving path following for multiple fixed-wing unmanned aerial vehicles with speed constraints," *Automatica*, vol. 100, pp. 82–89, Feb. 2019.

[12] O. Mofid, S. Mobayen, C. Zhang, and B. Esakki, "Desired tracking of delayed quadrotor UAV under model uncertainty and wind disturbance using adaptive super-twisting terminal sliding mode control," *ISA Trans.*, vol. 123, pp. 455–471, Apr. 2022.

[13] J. Wang, L. Han, X. Dong, Q. Li, and Z. Ren, "Distributed sliding mode control for time-varying formation tracking of multi-UAV system with a dynamic leader," *Aerosp. Sci. Technol.*, vol. 111, Apr. 2021, Art. no. 106549.

[14] B. Li, W. Gong, Y. Yang, B. Xiao, and D. Ran, "Appointed fixed time observer-based sliding mode control for a quadrotor UAV under external disturbances," *IEEE Trans. Aerosp. Electron. Syst.*, vol. 58, no. 1, pp. 290–303, Feb. 2022.

[15] M. Pouzesh and S. Mobayen, "Event-triggered fractional-order sliding mode control technique for stabilization of disturbed quadrotor unmanned aerial vehicles," *Aerosp. Sci. Technol.*, vol. 121, Feb. 2022, Art. no. 107337.

[16] O. Mofid and S. Mobayen, "Adaptive sliding mode control for finite-time stability of quad-rotor UAVs with parametric uncertainties," *ISA Trans.*, vol. 72, pp. 1–14, Jan. 2018.

[17] L. Yu, G. He, X. Wang, and S. Zhao, "Robust fixed-time sliding mode attitude control of tilt trirotor UAV in helicopter mode," *IEEE Trans. Ind. Electron.*, vol. 69, no. 10, pp. 10322–10332, Oct. 2022.

[18] Z. Gu, T. Yin, and Z. Ding, "Path tracking control of autonomous vehicles subject to deception attacks via a learning-based event-triggered mechanism," *IEEE Trans. Neural Netw. Learn. Syst.*, vol. 32, no. 12, pp. 5644–5653, Dec. 2021.

[19] S. Hu, D. Yue, X. Chen, Z. Cheng, and X. Xie, "Resilient H_∞ filtering for event-triggered networked systems under nonperiodic DoS jamming attacks," *IEEE Trans. Syst. Man Cybern.: Syst.*, vol. 51, no. 3, pp. 1392–1403, Mar. 2021.

[20] Z. Gu, X. Sun, H. K. Lam, D. Yue, and X. Xie, "Event-based secure control of T–S fuzzy based 5-DOF active semi-vehicle suspension systems subject to DoS attacks," *IEEE Trans. Fuzzy Syst.*, vol. 30, no. 6, pp. 2032–2043, Jun. 2022.

[21] F. Yang, Z. Gu, and S. Yan, "Switched event-based control for nonlinear cyber-physical systems under deception attacks," *Nonlinear Dyn.*, vol. 106, no. 3, pp. 2245–2257, Nov. 2021.

[22] F. Qu, E. Tian, and X. Zhao, "Chance-constrained H_∞ state estimation for recursive neural networks under deception attacks and energy constraints: The finite-horizon case," *IEEE Trans. Neural Netw. Learn. Syst.*, to be published, doi: 10.1109/TNNLS.2021.3137426.

[23] T. Alladi, N. G. Bansal, V. Chamola, and M. Guizani, "SecAuthUAV: A novel authentication scheme for UAV-ground station and UAV-UAV communication," *IEEE Trans. Veh. Technol.*, vol. 69, no. 12, pp. 15068–15077, Dec. 2020.

[24] X. Xu, X. Li, P. Dong, Y. Liu, and H. Zhang, "Robust reset speed synchronization control for an integrated motor-transmission powertrain system of a connected vehicle under a replay attack," *IEEE Trans. Veh. Technol.*, vol. 70, no. 6, pp. 5524–5536, Jun. 2021.

[25] P. Ramanan, D. Li, and N. Gebraeel, "Blockchain-based decentralized replay attack detection for large-scale power systems," *IEEE Trans. Syst. Man Cybern.: Syst.*, vol. 52, no. 8, pp. 4727–4739, Aug. 2022.

[26] H. Pu, L. He, C. Zhao, D. K. Yau, P. Cheng, and J. Chen, "Fingerprinting movements of industrial robots for replay attack detection," *IEEE Trans. Mobile Comput.*, vol. 21, no. 10, pp. 3629–3643, Oct. 2022.

[27] Z. Wu, E. Tian, and H. Chen, "Covert attack detection for LFC systems of electric vehicles: A dual time-varying coding method," *IEEE/ASME Trans. Mechatronics*, to be published, doi: 10.1109/TMECH.2022.3201875.

[28] J. Liu, T. Yin, D. Yue, H. R. Karimi, and J. Cao, "Event-based secure leader-following consensus control for multiagent systems with multiple cyber attacks," *IEEE Trans. Cybern.*, vol. 51, no. 1, pp. 162–173, Jan. 2021.

[29] D. Yue, E. Tian, and Q. Han, "A delay system method for designing event-triggered controllers of networked control systems," *IEEE Trans. Autom. Control*, vol. 58, no. 2, pp. 475–481, Feb. 2013.

[30] S. Yan, M. Shen, S. K. Nguang, and G. Zhang, "Event-triggered H_∞ control of networked control systems with distributed transmission delay," *IEEE Trans. Autom. Control*, vol. 65, no. 10, pp. 4295–4301, Oct. 2020.

[31] A. Seuret and F. Gouaisbaut, "Wirtinger-based integral inequality: Application to time-delay systems," *Automatica*, vol. 49, no. 9, pp. 2860–2866, Sep. 2013.

[32] L. Wei, M. Chen, and T. Li, "Disturbance-observer-based formation-containment control for UAVs via distributed adaptive event-triggered mechanisms," *J. Franklin Inst.*, vol. 358, no. 10, pp. 5305–5333, Jul. 2021.

[33] S. Yan, Z. Gu, and S. K. Nguang, "Memory-event-triggered H_∞ output control of neural networks with mixed delays," *IEEE Trans. Neural Netw. Learn. Syst.*, vol. 33, no. 11, pp. 6905–6915, Nov. 2022.

[34] X. Xie, D. Yue, J. H. Park, and J. Liu, "Enhanced stabilization of discrete-time Takagi-Sugeno fuzzy systems based on a comprehensive real-time scheduling model," *IEEE Trans. Syst. Man Cybern.: Syst.*, vol. 52, no. 2, pp. 881–892, Feb. 2022.

[35] B. Luo, T. Huang, and D. Liu, "Periodic event-triggered suboptimal control with sampling period and performance analysis," *IEEE Trans. Cybern.*, vol. 51, no. 3, pp. 1253–1261, Mar. 2021.

[36] X. Meng and T. Chen, "Optimal sampling and performance comparison of periodic and event based impulse control," *IEEE Trans. Autom. Control*, vol. 57, no. 12, pp. 3252–3259, Dec. 2012.

[37] A. Cuenca, D. J. Antunes, A. Castillo, P. Garcia, B. A. Khashooei, and W. Heemels, "Periodic event-triggered sampling and dual-rate control for a wireless networked control system with applications to UAVs," *IEEE Trans. Ind. Electron.*, vol. 66, no. 4, pp. 3157–3166, Apr. 2019.

[38] W. Cai, J. She, M. Wu, and Y. Ohyama, "Disturbance suppression for quadrotor UAV using sliding-mode-observer-based equivalent-input-disturbance approach," *ISA Trans.*, vol. 92, pp. 286–297, Sep. 2019.

[39] X. Xie, Q. Zhou, D. Yue, and H. Li, "Relaxed control design of discrete-time Takagi–Sugeno fuzzy systems: An event-triggered real-time scheduling approach," *IEEE Trans. Syst. Man, Cybern.: Syst.*, vol. 48, no. 12, pp. 2251–2262, Dec. 2018.

[40] W. Song, J. Wang, S. Zhao, and J. Shan, "Event-triggered cooperative unscented Kalman filtering and its application in multi-UAV systems," *Automatica*, vol. 105, pp. 264–273, Jul. 2019.

[41] S. Shao, M. Chen, J. Hou, and Q. Zhao, "Event-triggered-based discrete-time neural control for a quadrotor UAV using disturbance observer," *IEEE/ASME Trans. Mechatronics*, vol. 26, no. 2, pp. 689–699, Apr. 2021.

[42] X. Lin, J. Liu, Y. Yu, and C. Sun, "Event-triggered reinforcement learning control for the quadrotor UAV with actuator saturation," *Neurocomputing*, vol. 415, pp. 135–145, Nov. 2020.

[43] J. Liu, L. Wei, X. Xie, E. Tian, and S. Fei, "Quantized stabilization for T–S fuzzy systems with hybrid-triggered mechanism and stochastic cyber-attacks," *IEEE Trans. Fuzzy Syst.*, vol. 26, no. 6, pp. 3820–3834, Dec. 2018.

[44] Z. Gu, D. Yue, J. H. Park, and X. Xie, "Memory-event-triggered fault detection of networked IT2 T–S fuzzy systems," *IEEE Trans. Cybern.*, to be published, doi: 10.1109/TCYB.2022.3155755.

Tingting Yin received the B.S. degree in network engineering from the Nanjing University of Posts and Telecommunications, Nanjing, China, in 2017, and the M.S. degree in software engineering from the Nanjing University of Finance and Economics, Nanjing, China, in 2020. She is currently working toward the Ph.D. degree with the College of Mechanical and Electronic Engineering, Nanjing Forestry University, Nanjing, China. Her research interests include cyber-physical systems, multi-agent systems, and T–S fuzzy systems.

Zhou Gu (Member, IEEE) received the B.S. degree in automation from North China Electric Power University, Beijing, China, in 1997, and the M.S. and Ph.D. degrees in control science and engineering from the Nanjing University of Aeronautics and Astronautics, Nanjing, China, in 2007 and 2010, respectively. From September 1999 to January 2013, he was with the School of Power engineering, Nanjing Normal University as an Associate Professor. He is currently a Professor with Nanjing Forestry University, Nanjing, China. His research interests include networked control systems, time-delay systems, reliable control, and their applications.

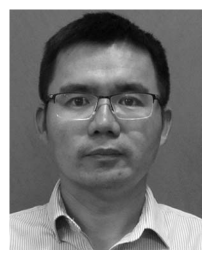

Xiangpeng Xie (Member, IEEE) received the B.S. and Ph.D. degrees in engineering from Northeastern University, Shenyang, China, in 2004 and 2010, respectively. From 2012 to 2014, he was a Postdoctoral Fellow with the Department of Control Science and Engineering, Huazhong University of Science and Technology, Wuhan, China. He is currently a Professor with the Institute of Advanced Technology, Nanjing University of Posts and Telecommunications, Nanjing, China. His research interests include fuzzy modeling and control synthesis, state estimations, optimization in process industries, and intelligent optimization algorithms.